Use of synthetic aperture radar polarimetry to characterize wetland targets of Keoladeo National Park, Bharatpur, India

Parul Patel[1,*], Hari Shanker Srivastava[2] and Ranganath R. Navalgund[1]

[1]Space Applications Centre, Indian Space Research Organization, Satellite Road, Ahmedabad 380 015, India
[2]Regional Remote Sensing Service Centre, Indian Space Research Organization, IIRS Campus, 4 Kalidas Road, Dehradun 248 001, India

Timely and accurate information about various habitats of a wetland ecosystem is necessary for the assessment, monitoring and management of a wetland. In this article, the state-of-the-art Polarimetric Synthetic Aperture Radar (PolSAR) data have been analysed to characterize various components of a wetland ecosystem. SAR polarimetry has received negligible attention in India, mostly owing to lack of data over the Indian sub-continent. With a recent DLR-ESAR (Experimental-SAR) flight over India, it was possible to conduct a detailed, planned experiment to explore the potentials of SAR polarimetry. This study has been carried out using fully polarimetric, multi-frequency DLR–ESAR data over parts of a world heritage and Ramsar site, the Keoladeo National Park, Bharatpur, India. Scattering models based on physical principles have been applied to characterize the wetland targets like open-water habitat, various types of aquatic vegetation with or without standing water, along with various species of forested areas. Entropy, alpha angle and anisotropy have been derived by performing eigen vector-based target decomposition on L- and P-bands fully polarimetric SAR data, enabling us to understand the differences in wetland targets in terms of their scattering behaviour at the L- and P-bands. A significant outcome of this study is that it explores and demonstrates the potential of the state-of-the-art technique of PolSAR for characterizing scattering behaviour of various components of a wetland ecosystem, which is a less explored application of SAR, particularly in the Asian countries.

Keywords: Polarimetric decomposition, Radar polarimetry, Synthetic Aperture Radar, wetland.

RADAR data are the best suited for monitoring a wetland ecosystem due to its all weather capability and unique sensitivity to the textural, structural, geometrical and electrical properties of various components of a wetland ecosystem[1]. Synthetic Aperture Radar (SAR) technology has advanced significantly after the launch of the first operational SAR sensor in 1991, in terms of development of state-of-the-art Polarimetric SAR (PolSAR) and Polarimetric Interferometric SAR (PolInSAR) techniques. This has further enhanced the capabilities of SAR sensor as a whole to characterize and monitor a wetland ecosystem.

Apart from SAR backscatter, the phase of the SAR signal also contains a lot of information about the target properties. SAR interferometry, SAR polarimetry and polarimetric interferometry are the techniques that exploit information on the phase of the SAR signal along with that of the SAR backscatter. A unique technique, namely SAR tomography is also being employed for target parameter retrieval in terms of a 3D representation of the area being imaged[2]. Polarimetry interferometry is also an active area of research[3].

Fully polarimetric SAR acquires four channels to obtain the complete scattering matrix, wherein the signal is transmitted in two orthogonal polarizations and received at two orthogonal polarizations. Most of the SAR polarimetric work has been carried out using airborne SAR sensors capable of acquiring data in the fully polarimetric mode, owing to the unavailability of satellite polarimetric SAR data. More recently, polarimetric satellite SAR data are available to the user community like experimental product from L-band PALSAR and operational product from RADRSAT-2 SAR. India is also on the verge of launching C-band RISAT-1, its first indigenous SAR satellite sensor. RISAT-1 is capable of acquiring data in quad polarization and in circular polarimetric mode, which is the first of its kind[4].

SAR is a useful tool to characterize various targets of a wetland ecosystem, as it is not only sensitive to the dielectric, physical and geometric properties of various wetland habitats, but is also sensitive to the relative proportion and distribution of various scatterers within an area-extended target. This unique sensitivity of SAR backscatter to the distribution of dielectric and geometric discontinuities makes it one of the most suitable tools in characterizing various wetland targets. In general, a wetland ecosystem is made up of targets having a number of distinct dielectric as well as geometric discontinuities and it is more of a layered system. Distribution and relative proportion of various geometric and dielectric properties

*For correspondence. (e-mail: parul@sac.isro.gov.in)

of scatterers in an area-specific target like a wetland ecosystem are critical for its waterfowls and flora (both aquatic and terrestrial). When a wetland target is illuminated by SAR, the backscatter is a composite effect of the dielectric and geometric discontinuities present in the form of vegetation, understorey vegetation, moisture content of each of the vegetation constituents, and presence or absence of standing water along with moisture status underneath the vegetation cover. Apart from the standing water (waterlogged condition), soil moisture is one of the most important information required for the survival of a wetland ecosystem. SAR can play an important role in providing soil moisture information. A number of semi-empirical and empirical models have been developed using multi-incidence angle, multi-polarized and multi-frequency SAR data[5–13]. Forest plantation surrounding the wetland is also an important part of the wetland ecosystem, as birds and waterfowls use them for nesting and resting. SAR has also been used extensively to study forest plantation. Patel *et al.*[14] have evaluated the sensitivity of multi-frequency, multi-polarized SAR to plant density. Detection and mapping of forest density has also been done using SAR interferometric technique[15,16]. From the viewpoint of a wetland ecosystem, sensitivity of SAR backscatter towards moisture content of the soil can be used to find localities of high soil moisture zones, whereas sensitivity of SAR backscatter towards vegetation structure and vegetation moisture can be used to discriminate various species of aquatic vegetation. Sensitivity of SAR data towards vegetation parameters has been explored by many researchers. For example, Patel *et al.*[17] demonstrated that by proper selection of sensor parameters, plant parameters can be retrieved from the SAR backscatter. The application potential of SAR in wetland studies has been exploited using multi-polarized, multi-temporal, multi-incidence angle SAR data over the Keoladeo National Park[1,18]. Effect of inundation on SAR backscatter response at different frequencies has been studied by Ormsby *et al.*[19].

A number of approaches are available for parameter retrieval using SAR polarimetry. Polarization signature is the simplest technique to visualize the scattering mechanisms present in a scene. This can be studied from feature to feature to relate the signatures of known simple targets, making it possible to infer the type of scattering that is taking place. However, when pixels over an area are averaged, the net response contains components from more than one type of scatterer and noise as well. At the same time, these scattering components are additive, limiting their use for parameter retrieval. The concept of quadrature-polarization (or full polarization)[20] was introduced to the remote sensing community in the 1980s. Attempts were made to understand the scattering mechanisms present in the polarimetric data. Many procedures have been employed to study polarimetric response from a target[21,22]. An unsupervized classifier has been developed by Van Zyl *et al.*[20] which classifies the image pixels to odd-bounce, even-bounce and diffuse using a purely mathematical model. This is achieved by exploiting the difference of scattering behaviour in terms of the relative phase changes by 180° for every bounce of simple geometric structures. Freeman and Durden[23] have also developed physical-based models which estimate the percentage of each of the even, odd and diffuse scattering mechanisms present at each pixel of the image. However, when large variability exists in the data, apart from the mean scattering process that is involved during the interaction of PolSAR with the target, the other information that can be extracted from the polarimetric response of the target is the number of scattering mechanisms and the purity of the target response. Attempts have also been made to develop target vector decomposition in order to relate to the physical process that takes place when SAR interacts with the target[24].

The potential of SAR polarimetry has been explored for studying surface parameters like soil moisture, surface roughness, forested land, ocean targets, etc.[25–28]. Wetland targets typically have a layered structure with varying degree of moisture/water conditions underneath the grass structure. While the usefulness of SAR backscatter data has been well explored[1], fully polarimetric data which can provide a unique insight into the scattering mechanism of SAR with these targets are relatively less explored. This article presents the outcome of a study that attempts to characterize wetland targets in terms of their scattering mechanism. For this purpose first, eigen vector-based target vector decomposition is carried out[24] to arrive at the entropy (H), alpha angle (α) and anisotropy (A). These parameters are used to understand the polarimetric response of the L- and P-bands to study purity of the target, mean scattering mechanism and the number of scattering mechanisms involved for each of the wetland targets, followed by Wishart H, A, α-segmentation. Finally, a comparative evaluation of the scattering mechanism that a wetland target undergoes when intercepted by L- and P-bands obtained with the help of physical model-based target decomposition algorithm is carried out.

Data set and study area

The data used for the study are fully polarimetric L- and P-bands acquired by DLR E-SAR (Experimental-SAR) on 19 September 2004 over parts of Bharatpur District, Rajasthan[29]. The study area, i.e. Keoladeo National Park, Bharatpur, is a World Heritage and Ramsar site. Figure 1 shows the location map of the study area. The park harbours over 350 bird species and 27 mammals. It is an important staging ground for waterfowls and also to the rare and dwindling Siberian cranes. The study area has a tropical monsoon climate. The total area of the park is

about 29 km^2, of which about 8.32 km^2 is under water-spread. Within the aquatic vegetation area of the park, most of the region is under *Paspalaum distichum*. Many species use open-water habitats and localities of free-floating and emergent aquatic vegetation. Areas totally dominated by *P. distichum* are not preferred by many species, except for purple moorhen, Jacanas and few others. In the tree/shrub vegetation, a mixture of *Prosopis juliflora*, *Acacia nilotica* and *Salvodora* species dominate the park. A few patches of *Mitragyna parvifolia* and *Syzygium cumini* trees are also noted in the park. In some parts of the sanctuary, extensive occurrence of *Vetivera zizanoides* is noted. Thus, a large variability in terms of wetland targets was present in the study area for the experiment.

Methodology

The signals at the output of radar receivers are, by nature, due to a coherent integration of contributions from highly complex scattering mechanisms. When a PolSAR system transmits two orthogonal polarized signals, the interaction of the target transforms its polarization depending upon the target characteristics. Hence the polarimetric signature from a target strongly depends upon the actual scattering process. This is the reason why SAR polarimetry has a characteristic property to discriminate different scattering mechanisms that take place when a target interacts with the incoming signals. This, in turn, leads to possibilities to understand the scattering process which takes place using physical-based scattering models.

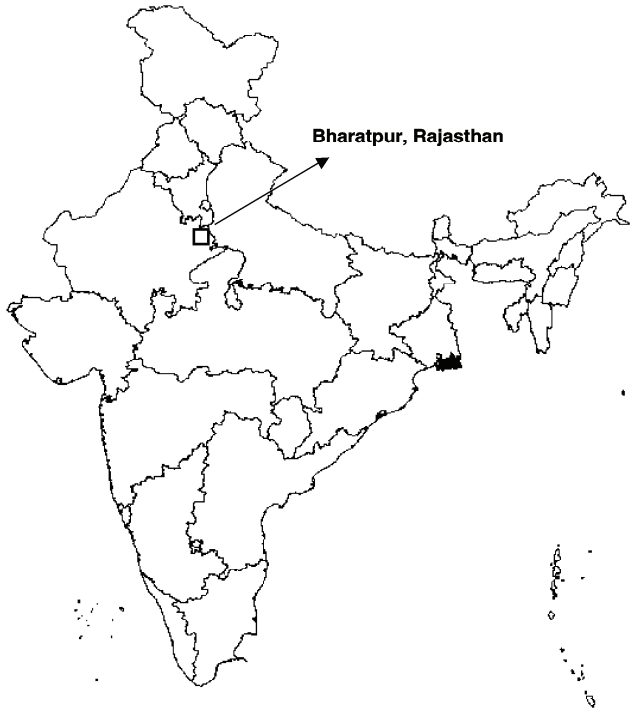

Figure 1. Location map showing the study area.

Polarimetric target decomposition is a technique that helps in understanding the scattering mechanism that is involved when a target interacts with SAR. This is an added advantage of SAR polarimetry over conventional SAR remote sensing technique. Coherent and non-coherent polarimetric target decomposition techniques have been developed[30]. Coherent decomposition expresses the scattering matrix [*S*], as a combination of the scattering responses of simpler objects. Coherent decomposition is more suitable for pure/point targets; hence its use is limited for distributed targets. Distributed scatterer can only be statistically characterized, due to the presence of speckle noise. Hence the non-coherent decomposition involves decomposing the coherency matrix. The coherency matrix, which is a second-order descriptor, can be achieved over a 3×3 window. In general, an image area consists of distributed targets. Hence non-coherent decomposition of the coherency matrix is preferred over coherent decomposition to characterize a given scene. In the present study, the coherency matrices of L- and P-bands have been decomposed using eigen vector-based decomposition algorithm. Once the eigen vector-based decomposition is achieved, the entropy, alpha angle and anisotropy are computed to arrive at the scattering mechanism using Wishart *H*–alpha anisotropy segmentation of the L- and P-bands, as described in the following sub-sections.

Entropy, alpha and anisotropy

SAR polarimetric analysis leading to the computation of entropy (H), anisotropy (A) and alpha angle (α), is useful for understanding the scattering process. To arrive at the values of H, A and α first, the coherency matrix [T] is obtained from the target scattering matrix [s] as follows.

$$[s] = \begin{bmatrix} S_{\mathrm{HH}} & S_{\mathrm{HV}} \\ S_{\mathrm{VH}} & S_{\mathrm{VV}} \end{bmatrix}.$$

From the scattering matrix, the Pauli scattering vector $\vec{k}$ is obtained as

$$\vec{k} = 1/2[S_{\mathrm{HH}} + S_{\mathrm{VV}} S_{\mathrm{HH}} - S_{\mathrm{VV}} 2S_{\mathrm{HV}}]^T. \quad (1)$$

From the Pauli scattering vector, the coherency matrix is obtained as

$$[T] = \vec{k}\vec{k}^*. \quad (2)$$

Once [T] is obtained, eigen vector decomposition is performed over the coherency matrix T as[24]

$$[T] = \lambda_1(\vec{e}_1\vec{e}_1^*) + \lambda_2(\vec{e}_2\vec{e}_2^*) + \lambda_3(\vec{e}_3\vec{e}_3^*), \quad (3)$$

where λ_i are the eigen values of the coherency matrix[21]. The eigen vectors $\vec{e}_i$ are as given by

$$\vec{e}_i = \begin{bmatrix} \cos\alpha_i e^{i\phi_{i1}} \\ \sin\alpha_i \cos\beta_i e^{i\phi_{i2}} \\ \sin\alpha_i \sin\beta_i e^{i\phi_{i3}} \end{bmatrix}. \quad (4)$$

ϕ_is are the phase differences, and α_i and β_i are the rotation angles.

After eigen vector decomposition of the coherency matrix the entropy (H), which is a measure of the randomness of the scattering process, is deduced from the eigen vectors as

$$H = -P_1 \log P_1 - P_2 \log P_2 - P_3 \log P_3, \quad (5)$$

where

$$P_i = \frac{\lambda_i}{\sum_{j=1}^{3} \lambda_j}. \quad (6)$$

Entropy is a measure that indicates the randomness in the target vector. For pure targets the entropy equals to 0, whereas for distributed target entropy equals 1.

The alpha angle (α) is obtained from the α_i angle of each of the eigen vectors as follows:

$$\bar{\alpha} = \sum_{i=1}^{3} P_i \alpha_i. \quad (7)$$

α angle is indicative of the average or dominant scattering mechanism. It describes the dominance of the scattering mechanism in terms of volume, double bounce or surface scattering. The lower limit of $\alpha = 0°$ indicates surface scattering, $\alpha = 45°$ indicates dipole or volume scattering, while the upper limit of $\alpha = 90°$. represents a dihedral reflector or multiple scattering.

The anisotropy A is obtained using the second and third eigen values as

$$A = \frac{\lambda_2 - \lambda_3}{\lambda_2 + \lambda_3}. \quad (8)$$

Anisotropy (A) is a measure of the differences in the secondary scattering mechanism. Low value of anisotropy indicates one dominant scattering mechanism with less significant second and third scattering mechanisms, whereas a high value of anisotropy indicates two dominant scattering mechanisms with equal probability and with a less significant third scattering mechanism.

Wishart entropy alpha anisotropy classification

The model suggested by Cloude and Pottier[24] has been employed to arrive at entropy, alpha and anisotropy segmentation to segment the image in terms of its scattering mechanism. The entropy–alpha space and the associated physical scattering in terms of mean scattering process and the high or low values of entropy indicates the randomness of the target[25]. The entropy–alpha space divides the target response into eight classes in accordance to the mean scattering process and the randomness of the scattering process. The entropy–alpha space is not able to distinguish the number of scattering mechanisms and their relative dominance. By introducing anisotropy which is a measure of the number of dominant scattering mechanisms involved in the scattering process, it is feasible to achieve better discrimination between the different scattering classes. Anisotropy is particularly useful to discriminate scattering mechanisms with different eigen-value distributions but with similar intermediate entropy values. When the entropy values for two clusters are the same, a high anisotropy value indicates two dominant scattering mechanisms with equal probability and a less significant third mechanism, whereas a low anisotropy value indicates a dominant first scattering mechanism and two non-negligible secondary mechanisms with equal importance. Segmentation of the image into a total of 16 classes indicating the mean scattering process, the purity of the target under consideration and the number of scattering mechanisms along with their dominance is achieved using entropy–alpha–anisotropy classification. However, the fixed linear decision boundaries in the H–α–A plane may affect the classifier performance for those pixels which fall on the boundary of the decision plane. Hence such boundary pixels may be wrongly assigned to a scattering class. This is because although H, α and A are computed using fully polarimetric data, these three parameters do not represent the complete polarimetric information. Therefore, there is a need to adopt segmentation procedures that take into consideration the whole coherency matrix statistics to overcome the limitations of purely decision-based classifiers. Statistical segmentation procedure with initial clusters based on the physical interpretation of the scattering phenomenon arrived at using H, α and A significantly enhances the performance of statistical segmentation schemes. While the target vector is complex normal, $N_C(0, [\Sigma])$, the n-look covariance matrix $[C]$ follows a complex Wishart distribution, $W_C(0, [\Sigma])$. Once the physical model-based eight classes are arrived at using the H–α decision plane, the class coherency matrix maximum likelihood (ML) estimate is computed for each cluster. Pixels are then assigned to a class according to the ML distance measure. Once the physical model-based eight classes are refined in accordance with the Wishart maximum likelihood distance, we get eight stable classes. These are further split into 16 classes based upon the value of anisotropy being less than or greater than 0.5 for a given pixel. These 16 classes are once again subjected to a second Wishart ML segmentation procedure to arrive at 16 stable classes. Thus, by combining the statistical

segmentation technique with initial classes as those arrived at by the H–α–A plane, the information content of the whole coherency matrix is utilized to enhance the classifier.

Results and discussions

Entropy, anisotropy and alpha angle for L- as well as P-bands fully PalSAR data were obtained using eqs (5), (7) and (8). The entropy for L- and P-bands is given in Figure 2. The α angle for L- and P-bands is given in Figure 3 and the anisotropy for L- and P-bands is given in Figure 4. The entropy, alpha angle and anisotropy are colour-coded in accordance to the limits that characterize the scattering process. For example, the entropy for L- and P-bands given in Figure 2 has been colour-coded to identify the areas having entropy less than 0.5 and more than 0.5. With the colour code, a reader can directly compare the behaviour of a target in L- and P-bands for each of the Figures 2–4. Once entropy, anisotropy and α angle are obtained for the L- and P-bands, segmentation based upon the eigen vector-based decomposition, namely Wishart H–α is carried out to arrive at eight segments. The segmentation showing different scattering mechanisms using Wishart H–α classification as described earlier for the L- and P-bands is given in Figure 5. The eight segments arrived at using Wishart H–α classification procedure are further subjected to anisotropy being less than or greater than 0.5 yielding 16 segments, which are further refined using Wishart H–A–α (Figure 6). Here, the entropy anisotropy and α angle behaviour of the L- and P-bands are first compared followed by studying Figures 5 and 6, for comparing the scattering mechanism that is experienced by the targets when intercepted by the L-band and how the same target exhibits a different scattering mechanism when intercepted by the P-band.

Comparison of entropy, anisotropy and α angle for L- and P-bands

The impact of frequency at which the target is being observed on entropy values for the L- and P-bands is clear

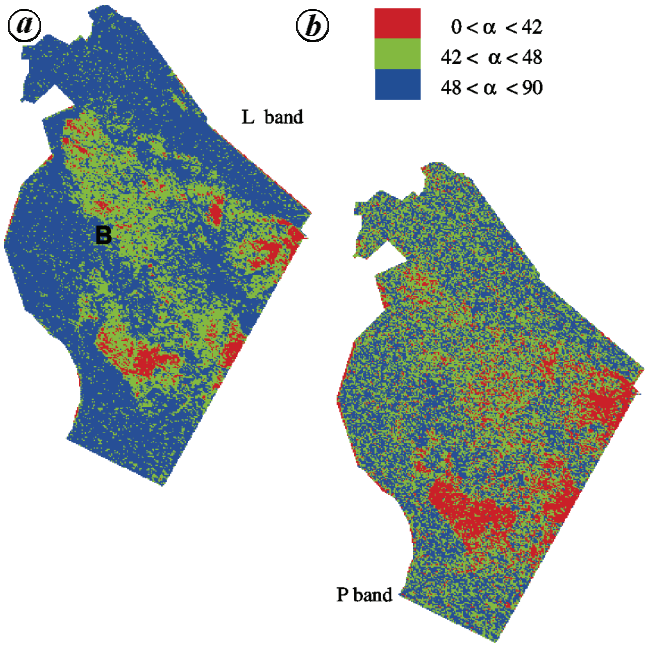

Figure 3. Alpha angle for L-band (***a***) and P-band (***b***).

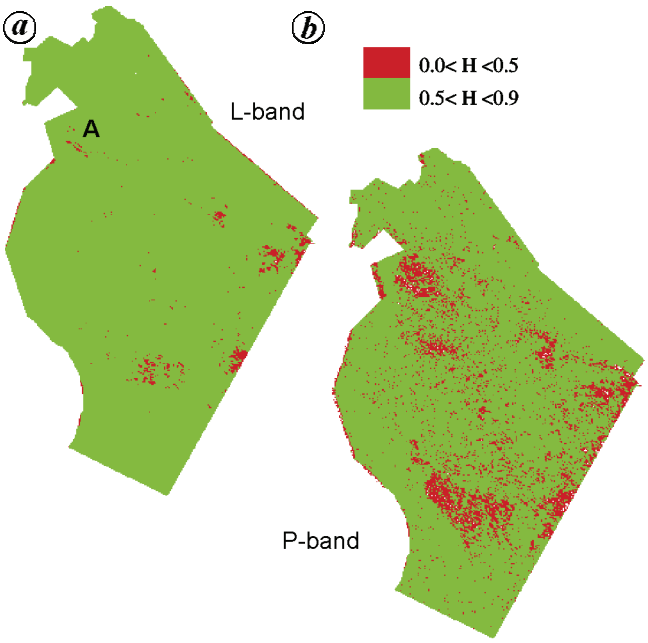

Figure 2. Entropy H for L-band (***a***) and P-band (***b***).

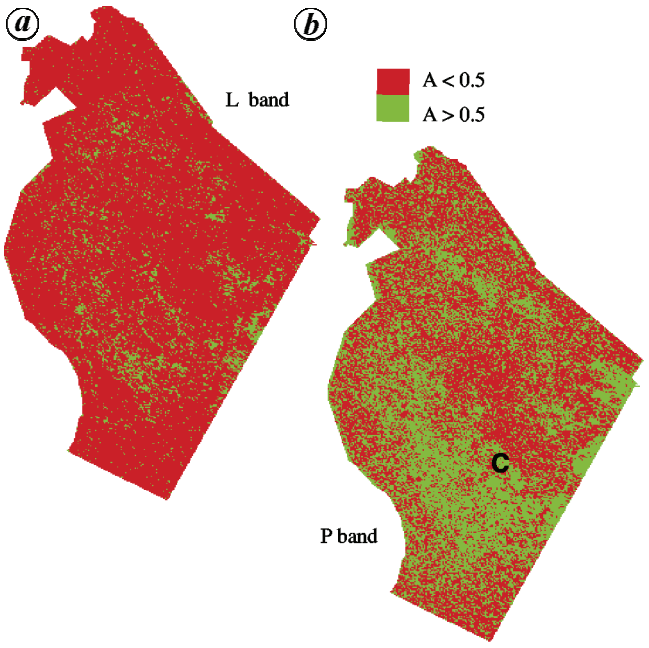

Figure 4. Anisotropy (A) for L-band (***a***) and P-band (***b***).

when one studies the target near marked position A in Figure 2. The area near A comprises of wetland area. For the P-band, the wetland area (appearing in red colour in Figure 2 *b*) acts more as a pure target, whereas for the L-band this target (appearing in green colour in Figure 2 *a*) is observed to be relatively distributed, indicating that randomness is higher in the L-band polarimetric response at location A. In Figure 3, an area dominated by grass is marked with B. While studying the α angle for location B for L- and P-bands, one can observe that while for the L-band the value of mean α angle is lower than 42°, indicating the scattering process to be single-bounce surface scattering, for the P-band this feature yields a value of α between 42° and 45°, indicating a volume scattering component in the scattering process. The response of L- and P-bands in terms of α angle indicates that while the grass yielded surface scattering for the L-band, for the P-band it was almost transparent, the P-band senses the moisture variations underneath giving rise to volume scattering.

The impact of the number of dominant scattering mechanisms in both the images due to variation in the frequency of observation is clear by studying the anisotropy values for both the images for L- and P-bands. As can be observed near location C in Figure 4, it is dominated by mixed vegetation with varying profile soil moisture, the L-band is significantly low compared to the P-band, indicating mostly one dominant scattering mechanism with two non-negligible secondary scattering mechanisms for the L-band and mostly two dominant scattering mechanisms for the P-band, with a third less dominant scattering mechanism. This phenomenon is expected due to the higher penetration of the P-band, thus interacting with more components of the target under consideration.

Scattering mechanism observed by Wishart H–α and Wishart H–α–A scheme of L- and P-bands

When one studies the result of Wishart *H–α* and Wishart *H–α–A* classification for the L and P bands given in Figures 5 and 6, a number of wetland and upland categories can be observed in different colour codes indicating different scattering behaviour. The colour code given in Figure 5 indicates the nature of the scattering mechanism and the randomness of the target, whereas apart from giving this information, the colour code in Figure 6 also indicates whether the dominant scattering mechanism experienced by the target is one or two. Thus, a yellow colour in Figure 5 represents the scattering mechanism to be that coming from a pure target undergoing double reflection, whereas a magenta colour represents a scattering mechanism from a distributed target having single reflection. Similarly in Figure 6, which has 16 categories, with each of the eight categories observed in Figure 5 split into two categories depending upon the anisotropy values as

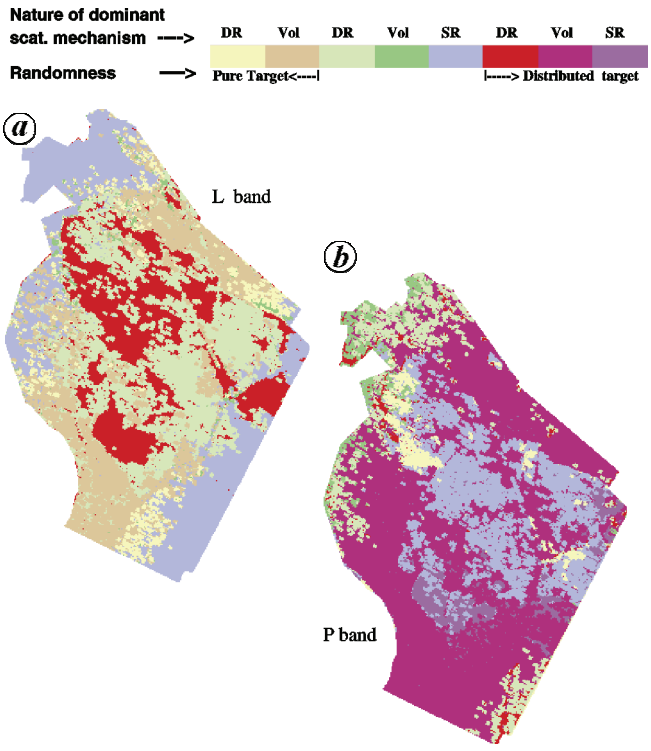

Figure 5. Wishart *H–α* classified output for L-band (***a***) and P-band (***b***).

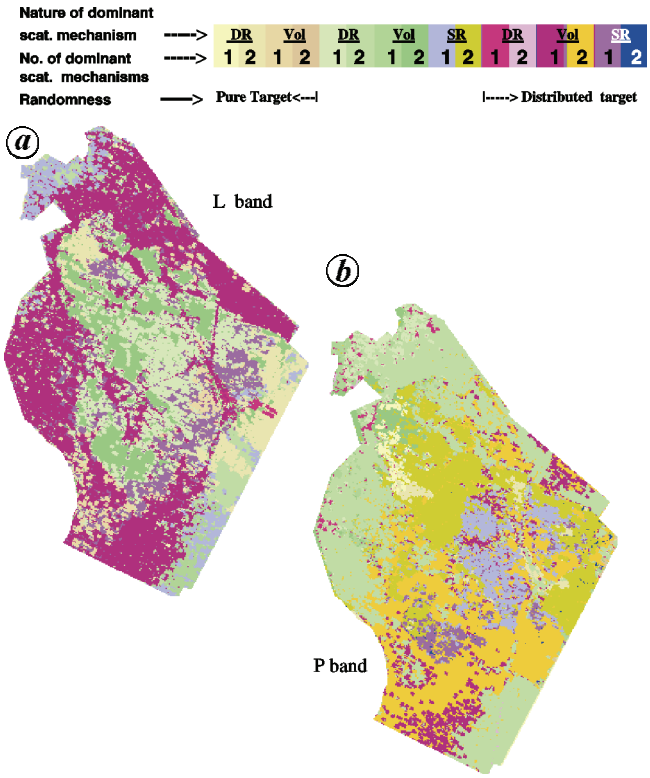

Figure 6. Wishart *H–α–A* classified output for L-band (***a***) and P-band (***b***).

Table 1. General distribution of scattering mechanism for major categories as detected by Wishart *H–α–A* classification scheme

Category	Frequency	Randomness of scattering process															
		Pure				Semi distributed						Distributed					
		Mean scattering process															
		DR		Vol		DR		Vol		SR		DR		Vol		SR	
		Number of dominant scattering mechanisms															
		1	2	1	2	1	2	1	2	1	2	1	2	1	2	1	2
Water	L															*	
	P										*						
Paspalaum distichum with underlying water	L		*														
	P	*															
Paspalaum distichum with underlying saturated soil	L					*											
	P		*														
Paspalaum distichum with underlying highly moist soil	L					*											
	P										*						
Paspalaum distichum with underlying moist soil	L					*											
	P									*							
Prosopis juliflora (young)	L													*			
	P													*			
Prosopis juliflora (old)	L							*									
	P						*										
Mixed dense jungle	L								*								
	P					*											
Acacia nilotica	L							*									
	P						*										
Syzygium cumini and *Mitragyna parvifolia*	L			*													
	P						*										

Dr, Double reflection; Vol, volume; SR, Single reflection.

described earlier, a yellow colour represents double reflection from a pure target having one dominant scattering mechanism and two non-negligible secondary scattering mechanisms. Whereas in Figure 6, the blue colour represents a distributed target with single reflection and having two dominant scattering mechanisms and a less dominant third scattering mechanism. The wetland area within the study area was dominated by open-water habitat and aquatic vegetation, namely *P. distichum* with varying underlying conditions like flooded water, wet soil and moist soil. In the upland area of study, there exists *P. juliflora*, *A. nilotica*, *S. cumini* and *M. parvifolia*. Table 1 provides the scattering mechanism that these wetland and upland targets undergo when intercepted by L- or P-bands as observed in Figure 6 using Wishart *H–α–A* classification scheme. The colour code with which the scattering mechanism for these categories are coded in Figure 6 is also reproduced in Table 1 to enable the reader to relate the scattering mechanisms of various categories. Table 1 and Figure 6 reveal that, in general the scattering mechanism identified by the Wishart *H–α* classification which has been further fine-tuned to more stable classes after the Wishart *H–α–A* classification is in accordance with the expected interaction that would take place between a given target and the SAR signal depending upon the target characteristics and frequency with which it is intercepted. For example, a comparison of the L- and P-bands shows that Wishart *H–α–A* identify open water as a distributed target with single bounce as the scattering mechanism for the L-band whereas the P-band experiences a scattering mechanism for water as that of a single-bounce reflection from a semi-distributed target. *P. distichum* with standing water underneath is categorized as having undergone a double reflection from a pure target for P- and L-bands. L-band experiences two dominant scattering mechanisms whereas the P-band experiences a single dominant scattering mechanism. As the underlying soil conditions vary from standing water to soil with varying amount of moisture content, the scattering mechanism that takes place also varies with frequency. For example, whereas the L-band experiences a double reflection from a pure target for *P. distichum* with saturated, highly moist to moist soil, the P-band with saturated soil conditions undergoes a double

reflection from a semi-distributed target. For all the other moisture conditions underneath, *P. distichum* results in scattering mechanism from that of a semi-distributed target with single bounce for the L-band, whereas for the P-band high moist and moist soil condition underneath *P. distichum* results in a scattering mechanism from that of semi-distributed target with two and one dominant scattering mechanism respectively.

For different categories in the upland areas covered with *P. juliflora*, *A. nilotica*, *S. cumini* and *M. parvifolia* and mixed dense jungle, the scattering mechanisms identified using Wishart H–α–A scheme were mostly those coming from double reflection at P-band from semi-distributed target while at L-band, *A. nilotica* and mixed dense jungle resulted in volume scattering owing mostly to the limited penetration of the L-band, as compared to P-band, through the thick canopy, which is in accordance with the expected scattering process. Thus for different categories, a detailed information on the scattering mechanism experienced by the target at L- and P-bands can be compared by studying Figure 6 and Table 1. Thus the scattering process inferred from the polarimetric target vector of various wetland features using physical scattering model-based Wishart H–α–A segmentation scheme was found to be in accordance with the expected frequency dependence of penetration within vegetation layer and the soil/water layer underneath the vegetation.

Conclusion

In this study, wetland targets of the Keoladeo National Park have been characterized using SAR polarimetry. The study provides an insight into the scattering mechanism of various wetland targets along with the surrounding forest plantation using eigen vector-based target polarimetric decomposition which enables to describe the mean scattering process, the randomness of the target as well as the number of dominant scattering mechanisms, which is not feasible to infer with conventional SAR remote sensing. A comparative evaluation of the L- and P-bands based upon entropy, anisotropy and alpha angle highlighted difference in polarimetric response of a variety of wetland targets with varying surface conditions underneath due to the difference in frequency of observation. Scattering behaviour obtained using Wishart H–α–A classification has been compared for different wetland targets for their scattering mechanisms, as observed for the L- and P-bands. The results here indicate that SAR polarimetric physical-based scattering models are useful to understand the scattering process that takes place when a target interacts with SAR using fully PolSAR data.

1. Srivastava, H. S., Patel, P., Sharma, K. P. and Krishnamurthy, Y. V. N., Explored and demonstrated potential applications of multi-parametric synthetic aperture radar (SAR) in wetland studies in context of Keoladeo National Park, Bharatpur, India. In Second Annual Research Seminar on Keoladeo National Park (2ndARS-KNP), KNP, Bharatpur, 15 March 2009; www.ramsar.org/features/features_remote_ keoladeo.pdf
2. Reigber, A. and Moreira, A., First demonstration of SAR tomography using polarimetric airborne SAR data. *Trans. Geosci. Remote Sensing*, 2000, **38**, 2142–2152.
3. Ferro-Famil, L. E., Reigber, A., Pottier, E. and Boerner, W.-M., Multi-baseline polarimetric SAR data classification using the complex Wishart distribution and principal component analysis. In IEEE 2001 International Geoscience and Remote Sensing Symposium, IGARSS '01, 2001, vol. 6, pp. 2712–2714.
4. Misra, Tapan, Rana, S. S. and Shankara, K. N., Synthetic Aperture Radar payload of Radar Imaging Satellite (RISAT) of ISRO. In paper presented at the URSI-GA, Session F-08, Vigyan Bhavan, New Delhi, 26 October 2005.
5. Dubois, P. C., Van Zyl, J. and Engman, E. T., Measuring soil moisture with imaging radar. *IEEE Trans. Geosci. Remote Sensing*, 1995, **33**, 915–926.
6. Oh, Y., Sarabandi, K. and Ulaby, F. T., An empirical model and an inversion technique for radar scattering from bare soil surfaces. *IEEE Trans. Geosci. Remote Sensing*, 1992, **30**, 370–381.
7. Patel, P., Panigrahy, S. and Chakraborty, M., Performance of RADARSAT-1 extended low beam mode SAR data for soil moisture retrieval. *Asian J. Geoinf.*, 2002, **2**, 85–91.
8. Patel, P., Mohan, S., Sarma, S., Sutroddhar, A. K., Khawas, B. K. and Das, D. K., Evaluation of multi-incidence angle Radarsat SAR data for soil moisture estimation. In *Physical Methods of Soil Characterization*, Narosa Publishing House, New Delhi, 2001, pp. 133–140.
9. Srivastava, H. S., Patel, P. and Navalgund, R. R., How far SAR has fulfilled its expectation for soil moisture retrieval? In Proceedings of the 5th International Symposium on Asia-Pacific Remote Sensing, International Society for Optical Engineering, Goa, 13–17 November 2006, SPIE Digital Library (http://spiedl.aip.org), vol. 6410, Paper no. 641001, 2006, pp. 1–12.
10. Srivastava, H. S., Patel, P. and Navalgund, R. R., Incorporating soil texture in soil moisture estimation from Extended Low-1 Beam mode Radarsat-1 SAR data. *Int. J. Remote Sensing*, 2006, **27**, 2587–2598.
11. Srivastava, H. S., Patel, P., Manchanda, M. L. and Adiga, S., Use of multi-incidence angle Radarsat-1 SAR data to incorporate the effect of surface roughness in soil moisture estimation. *IEEE Trans. Geosci. Remote Sensing*, 2003, **41**, 1638–1640.
12. Srivastava, H. S., Patel, P., Manchanda, M. L. and Adiga, S., An attempt to incorporate the effect of crop cover in soil moisture estimation using multi-incidence angle Radarsat-1 SAR data. *Asian J. Geoinf.*, 2002, **2**, 33–40.
13. Srivastava, H. S., Patel, P., Sharma, Y. and Navalgund, R. R., Large-area soil moisture estimation using multi-incidence-angle RADARSAT-1 SAR data. *IEEE Trans. Geosci. Remote Sensing*, 2009, **47**, 2528–2535 (DOI: 10.1109/TGRS.2009.2018448).
14. Patel, P., Srivastava, H. S., Panigrahy, S. and Parihar, J. S., Comparative evaluation of the sensitivity of multi-polarized multi-frequency SAR backscatter to plant density. *Int. J. Remote Sensing*, 2006, **27**, 293–305.
15. Srivastava, H. S., Patel, P., Sharma, Y. and Navalgund, R. R., Detection and density mapping of forested areas using SAR interferometric technique. *Int. J. Geoinf.*, 2007, **3**, 1–10.
16. Srivastava, H. S., Patel, P. and Navalgund, R. R., Application potentials of Synthetic Aperture Radar Interferometry (InSAR) for land cover mapping and crop height estimation. *Curr. Sci.*, 2006, **91**, 783–788.
17. Patel, P., Srivastava, H. S. and Navalgund, R. R., Estimating wheat yield: an approach for estimating number of grains using cross-polarized ENVISAT-1 ASAR data. SPIE Digital Library, vol. 6410, Paper no. 641009, pp. 1–12; http://spiedl.aip.org

18. Srivastava, H. S., Prasad, S. N., Manchanda, M. L. and Adiga, S., Radar remote sensing applications in wetland habitat: I. A case study of Keoladeo National Park using multi-incidence angle RADARSAT-1 SAR data. In International Conference on Remote Sensing and GIS/GPS (ICORG), Spatial Information Technology, B.S. Publishers, Hyderabad, vol. II, 2001, pp. 87–92; http://www.geospatialtoday.com/articles/article_14.asp
19. Orsamby, J. P., Blanchard, J. P. and Blanchard, A. J., Detection of lowland flooding using active microwave systems. *Photogramm. Eng. Remote Sensing*, 1985, **51**, 317–328.
20. Van Zyl, J. J., Unsupervised classification of scattering behavior using radar polarimetry data. *IEEE Trans. Geosci. Remote Sensing*, 1989, **27**, 36–45.
21. Boerner, W. and Yamagushi, Y., Extra wideband polarimetry, interferometry and polarimetric interferometry in Synthetic Aperture Radar. Special issues on Advances in Radar Systems. *IEICE Trans. Commun.*, 2000, **E83-B(9)**, 1906–1915.
22. Qong, M., A new scattering mechanism enhancement scheme for polarimetric SAR images. *IEEE Trans. Geosci. Remote Sensing*, 2002, **40**, 2582–2592.
23. Freeman, A. and Durden, S. L., A three-component scattering model for polarimetric SAR data. *IEEE Trans. Geosci. Remote Sensing*, 1998, **36**, 963–973.
24. Cloude, S. R. and Pottier, E., An entropy based classification scheme for land applications of polarimetric SAR. *IEEE Trans. Geosci. Remote Sensing*, 1997, **35**, 68–78.
25. Irena, H., Pottier, E. and Cloude, S. R., Inversion of surface parameters from polarimetric SAR. *IEEE Trans. Geosci. Remote Sensing*, 2003, **41**, 727–739.
26. Mattia, F., Le Toan, T., Souyris, J. C., De Carolis, G., Floury, N., Posa, F. and Pasquariello, G., The effect of surface roughness on multi-frequency polarimetric SAR data. *IEEE Trans. Geosci. Remote Sensing*, 1997, **35**, 954–965.
27. Treuhaft, R. N. and Sequeira, P. R., Vertical structure of vegetated land surfaces from interferometric and polarimetric radar. *Radio Sci.*, 2000, **35**, 141–177.
28. Lee, J. S. *et al*., Polarimetric analysis and modeling of multifrequency SAR signatures from gulf stream fronts. *IEEE J. Ocean. Eng.*, 1998, **23**, 322–332.
29. Patel, P., Polarimetric SAR classification using physical based scattering mechanism: comparative evaluation of L and P bands. In Conference of Joint Experiment Project towards microwave Remote Sensing Data Utilisation, Ahmedabad, 15–16 May 2007, pp. 2-42–2-47.
30. Cloude, S. R. and Pottier, E., A review of target decomposition theorems in radar polarimetry. *IEEE Trans. Geosci. Remote Sensing*, 1996, **34**, 498–518.

ACKNOWLEDGEMENTS. P.P. and H.S.S. thank Dr J. S. Parihar, Deputy Director, Remote Sensing Applications Area and Dr Y. V. N. Krishnamurthy, Director, Regional Remote Sensing Service Centre (RRSSC) for their keen interest and encouragement. They also thank Dr M. Chakraborty, Group Director, Geo-Informatics and Techniques Development Group; Dr S. Mohan, Head, Advance Techniques Development Division and Dr K. P. Sharma, Head, RRSSC, Dehradun for encouragement and support.

Received 14 May 2008; revised accepted 23 June 2009